Terawatt CO_2 laser: a new tool for strong-field research

Igor Pogorelsky[a], Markus Babzien[a], Igor Pavlishin[a], Daniil Stolyarov[a], Vitaly Yakimenko[a], Peter Shkolnikov[b], Alexander Pukhov[c], Alexei Zhidkov[d], Victor T. Platonenko[e]
[a] Brookhaven National Lab., Upton, NY, USA
[b] Stony Brook Univ., Electrical. and Computer Engineering Dept., Stony Brook, NY, USA
[c] Inst. Theor. Physic I, Duesseldorf, Germany
[d] Univ. of Tokyo, Ibaraki, Japan
[e] M.V. Lomonosov Moscow State Univ., Moscow, Russia

ABSTRACT

We describe the physical principles and architecture of a multi-stage picosecond terawatt CO_2 laser system, PITER-I, operational at Brookhaven National Laboratory (BNL). The laser is a part of the DOE user's facility open for international scientific community. One of the prospective strong-field physics applications of PITER-I is the production of proton- and heavy-ion beams upon irradiating thin-film targets and gas jets. We discuss the possibilities for upgrading a CO_2 laser to a multi-terawatt femtosecond regime.

Keywords: CO_2 laser, proton beams, ion acceleration, ablation, plasma.

1. INTRODUCTION

Laser ablation is a broad subject that embraces a variety of applications from gentle restoration of ancient frescos to the laser propulsion. Contemporary ultra-fast lasers bring the ablation process to the next extreme wherein electrons and protons of matter are not just stripped apart but are violently accelerated in the form of directed relativistic beams. In this way, laser ablation intrudes into the area of the high-energy physics (HEP) - one of the most fundamental science disciplines that advance the frontiers of our understanding of matter and energy. At a more human scale, the HEP's mission is to provide compact particle accelerators for radiation treatment of tumors. Laser-driven proton- and ion-accelerators are likely candidates for this task.

Conventional RF or DC sources of an accelerating field approached their ceiling for the accelerating gradient at 100 MeV/m, defined by the vacuum breakdown. This is why scientists turned their attention to lasers that are the sources of the highest fields achieved in the laboratory environment. At a ready achievable intensity $I \approx 10^{16}$ W/cm^2, the transverse electric field reaches $E \approx 100$ GV/m (1000 times above conventional sources!). Laser-accelerator research explores methods of using such enormous transverse electromagnetic fields productively for high-gradient acceleration.

The BNL's Accelerator Test Facility (ATF) provides a setting to search for laser methods of particle acceleration. For this purpose, the ATF is equipped with a terawatt picosecond CO_2 laser and a 70 MeV high-brightness electron linac. Several world-class experiments and breakthrough results obtained over the last decade put the ATF among the leading facilities in advanced research on accelerator and radiation sources. The ATF's approach to laser-driven linear acceleration capitalizes on the fact that the CO_2 laser's wavelength offers a viable compromise between conventional RF linacs and optical laser drivers.

Further progress in laser-based particle acceleration research is anticipated primarily via using processes that start from electron oscillation in electromagnetic laser field E. CO_2 lasers also offer advantages in realizing these mechanisms. The intensity of electron oscillation is characterized by a ponderomotive potential

$$W_{osc} = e^2E^2 \Big/ 2m\omega^2 = mc^2a^2/2, \quad (1)$$

where e and m are, correspondingly, the electron charge and mass, ω is the laser frequency, and $a = eE/m\omega c$ is the dimensionless amplitude of the electromagnetic wave. At a given intensity, a CO_2 laser with a wavelength λ=10-μm achieves a 100 times higher ponderomotive potential than do 1-μm solid state lasers, opening the possibility of a attaining a proportional increase in a throughput of such processes as electron acceleration and x-ray generation. This again was demonstrated at the ATF where we achieved the brightest ever x-ray Thomson source[1] recently extended into

High-Power Laser Ablation VI, edited by Claude R. Phipps, Proc. of SPIE
Vol. 6261, 626118, (2006) · 0277-786X/06/$15 · doi: 10.1117/12.667811

a nonlinear regime[2]. A similar W_{osc} parameter is responsible for scaling up an ion acceleration that is achieved upon thin-foil ablation with ultra-fast high-energy lasers[3, 4].

Despite these advantages, CO_2 lasers are underutilized for advanced accelerator research compared with the more widely used solid-state lasers based on chirped pulse amplification (CPA). The main difficulty with building ultra-fast CO_2 lasers is that their gain spectrum is modulated with a molecular rotational structure so impeding amplification of broadband picosecond and femtosecond pulses. Fortunately, pressure broadening (above 10 atm) can alleviate this bandwidth limitation. Such high-pressure gas-laser technology is employed in the ATF's CO_2 laser system PITER-I (abbreviation from PIcosecond TERawatt). We describe here the design and operation of PITER-I and address the possibility of upgrading CO_2 lasers to femtosecond duration and petawatt peak power.

Among the most exciting upcoming applications in HEP is proton- and ion-acceleration where collimated relativistic particle beams originate from the rear surface of laser-irradiated foils and gas jets. CO_2 laser offers higher efficiency, better particle-beam quality and monochromaticity of ion- and proton acceleration compared with CPA lasers. The expected advantages are due to the stronger ponderomotive effects of a longer-wavelength CO_2 laser beam that generates the desired relativistic effects within a larger focal area and volume. This will further advance development of laser-driven proton- and ion-sources towards practical applications in science, medicine, and technology.

2. PICOSECOND TERAWATT CO_2 LASER "PITER-I"

The generation and amplification of a 1-ps radiation pulse requires an active medium with a 1 THz spectral bandwidth. Vibrational molecular bands in the CO_2 laser's gain spectrum extend over this range. However, vibrational bands are not continuous, but are composed of discrete transitions between multiple rotational sublevels.

Selection rules for a symmetric CO_2 molecule allow only those transitions where the rotational quantum number, J, changes by ±1. Those transitions constitute, correspondingly, the P- and the R-branches of vibrational bands with the central lines defined by the expressions:

$$\nu_P = \nu_0 + B_1 J(J+1) - B_2 (J+1)(J+2), \tag{2a}$$

$$\nu_R = \nu_0 + B_1 J(J+1) - B_2 (J-1)J, \tag{2b}$$

where ν_0 = 960.8 cm^{-1} for the 10-μm band, and =1063.6 cm^{-1} for the 9-μm band, B_1 and B_2 are, correspondingly, the rotational constants for the upper- and lower-vibrational levels ranging between 0.3866 cm^{-1} to 0.3899 cm^{-1} for the above bands. Taking into account an additional quantum selection rule ΔJ=2 between the adjacent spectral lines, the interline spacing $\Delta\nu$ is $\sim 4(B + \Delta B \times J)$ for the P-branch and $\sim 4(B - \Delta B \times J)$ for the R-branch. ΔB is a negative number equal to the difference between B-constants for upper and lower state. At the normal discharge temperature, the maximum line strength is at J~20 and a typical interline spacing varies between 1.4 cm^{-1} (38 GHz) for the 9R-branch to 1.8 cm^{-1} (55 GHz) for the 10P-branch.

At a gas pressure >30 torr, collision broadening of the individual line in the CO_2 laser spectrum defines its Lorentzian shape

$$\alpha_i(\nu) = \frac{\delta\nu/\pi}{(\nu - \nu_i)^2 + (\delta\nu)^2}, \tag{3}$$

with the FWHM bandwidth

$$\delta\nu = 5.97\left[\Psi_{CO_2} + 0.73\Psi_{N_2} + 0.64\Psi_{He}\right] P\left[\frac{300}{T}\right]^{1/2} \text{ (GHz)}, \tag{4}$$

where Ψ is a fraction of each gas component, P is the gas density in bars, and T is the absolute temperature (^{0}K). For a typical CO_2 -laser gas mixture CO_2:N_2:He=1:1:3, $\delta\nu$=5 MHz/torr. Comparing $\delta\nu$ with $\Delta\nu$, we conclude that lines within the 9R-branch overlap at P≈10 atmospheres, and within the 10P-branch at P≈15 atmospheres.

Fig. 1 shows a fragment of the gain spectrum (10R branch) for 1-atm and 10-atm CO_2 amplifiers. Estimating how ripples in the spectrum's envelope may affect a picosecond pulse amplification requires simulations that account for mutual interactions between the active medium and radiation pulse, and relaxation in the CO_2 energy levels. These processes are described by a system of Maxwell-Bloch equations.[5] Fig. 1 gives also examples of the numerical solution to these equations. We see that pulses as short as 1 ps can be amplified without distortion in a 10-atm CO_2 amplifier.

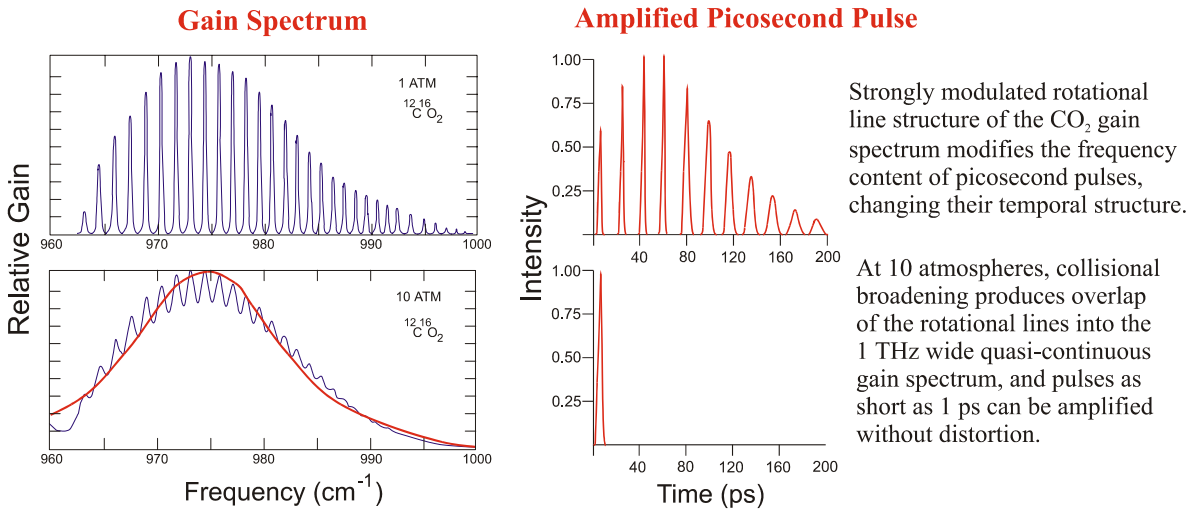

Figure 1: Simulations of the 10R-branch gain spectrum (left) and the amplified 1-ps seed pulse (right) in a CO_2 laser at 1 atm and 10 atm pressure. Smooth curve overlapping the 10-atm spectrum illustrates the 1-ps pulse bandwidth.

The initial exponential growth of the laser pulse propagating in the laser medium, which has a small-signal gain $g_0=\sigma\times N_{vj}$, where σ is the radiation transition cross-section ($\sigma=2\times10^{-19}$ cm^2 at 10 atm) and N_{vj} is the population inversion, saturates at a certain fluence W_s measured in J/cm^2. The W_s value normally is obtained via the best fit of the Franz-Nodvik equation

$$W(z)/W_s = \ln\{1+\exp(\beta_0 z)[\exp(W_0/W_s)-1]\} \qquad (5)$$

to a computer-simulated amplification curve obtained by direct solution of Maxwell-Bloch equations. Depending upon the input radiation spectrum and the ratio between the input pulse length τ and rotational relaxation time τ_R, which is 16 ps @ 10 atmospheres, W_s varies from $h\nu/2\sigma$ =30 mJ/cm^2 to $h\nu/2\sigma p(j_{\max})$ =500 mJ/cm^2, where $p(j_{\max})$=0.065 is the relative population of an individual rotational level at the maximum of the distribution. The maximum W_s value corresponds to a short, $\tau\lesssim1$ ps laser pulse that overlaps the entire vibrational band, extracting energy simultaneously from the whole manifold of rotational levels. The minimum W_s corresponds to $\tau\approx\tau_R$, the laser pulse that overlaps just one rotational line but is too short to allow its replenishment from neighboring levels during the passage of the pulse. With a further increase in τ, W_s rises back to the maximum as long as all rotational sublevels are depleted by rotational relaxation.

The multiple of $g_0\times W_s$ defines a specific excitation energy stored on the radiation-transition levels in the laser amplifier. For a typical small-signal gain coefficient, g_0=2.5 %/cm, the maximum specific stored energy available for extraction under saturation is $g_0\times W_s$ =7 J/l.

Hence, we see that creating a terawatt-class picosecond CO_2 laser is a two-fold task: building an amplifier of ≥10 atm pressure and several liters volume, and generating a seed laser pulse with $\tau<<\tau_R$.

Let us evaluate the problem of building high-pressure gas lasers pumped with electric discharge – the approach used in the ATF's laser system. A spatially uniform self-sustained glow discharge may exist only at Pd<25 torr cm, where d is an inter-electrode distance. At a higher pressure, an auxiliary source of ionization is needed that could be a UV-, x-ray, or electron-beam. Still, high pressure discharge generally is an unstable process, and it contracts into a streamer channel over times longer than $\tau_{disch}[\mu s]\approx3/P[\text{atm}]$, which is ~300 ns at 10 atm.

The pump pulse should supply sufficient stored energy for achieving the necessary small-signal gain and the required energy extraction. The efficiency of converting the pump energy into radiation for pulsed CO_2 lasers is 5-10%; this, in turn, defines the required energy deposition ~100 J/*l* atm. Thus, a 10-liter high-pressure amplifier will require several kilo-joules of energy deposition in a fast impedance-matched discharge.

This approach materialized in the laser amplifier PITER-I that Optoel Co. (St. Petersburg, Russia) built for the ATF.[6] This 10-atm gas laser, shown in Fig. 2, has an active length of 1 m, and V_a=10 *l* active volume, preionized with a built-in 100-kV x-ray tube, and energized with a ten-stage 1-MV Marx generator with a total stored energy of 8 kJ. A sharpening water capacitor converts the relatively slow 1-μs discharge from the Marx capacitor bank into a fast 250-ns discharge within the 10-cm wide x-ray preionized inter-electrode gap, thereby achieving a small-signal gain of g_0=2.5 %/cm. The multiple of $g_o \times W_s \times V_a \approx$70 J yields the stored energy available for extraction from the active medium in a single pass. However, the laser beam overlaps just a portion of the active volume and does not reach saturation. Consequently, the amplifier's output is limited to 10 J. The laser can operate at a repetition rate up to one pulse in ten seconds.

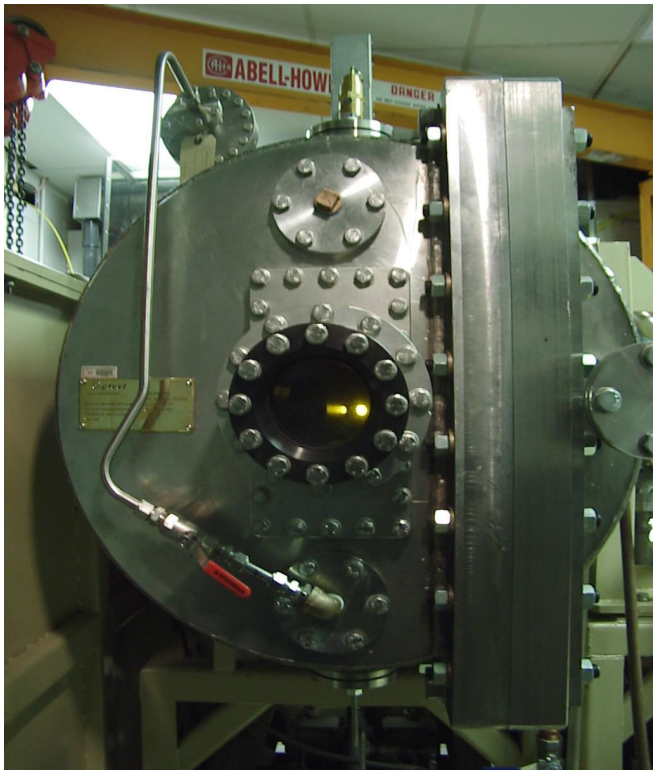

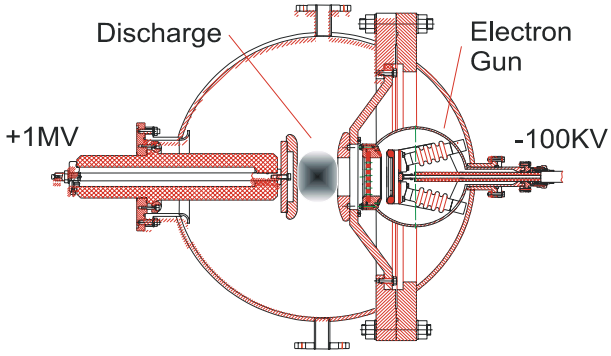

Amplifier cross-section diagram

Figure 2: A front view and a cross-section diagram of a high-pressure X-ray preionized CO_2 laser manufactured by Optoel Co. (St Petersburg, Russia). X-rays, produced by stopping 100-keV electrons on a Ta foil, penetrate through a mesh ground electrode into the discharge volume pumped by a 1-MV Marx generator.

PITER-I is the final and the most critical stage of the amplifier chain that raises the laser's peak power from the initial 100 kW to the 1 TW level. For a transition stage, we use a more conventional high-pressure CO_2 laser HP-5 manufactured by SDI Ltd. (Pretoria, S. Africa), shown in Fig.3. This laser features a 1.5×1.5×80 cm^3 active volume, UV-preionization, and fast, transverse, close-loop gas circulation through a catalytic converter. In the free-lasing regime, the HP-5 delivers a 1 J output at a 10 Hz repetition rate. We used the HP-5 laser in the regenerative amplifier mode, as described below.

Let us address the problem of producing picosecond CO_2 pulses. A CO_2 laser cannot generate picosecond pulses without having a shorter-wavelength laser. Several methods have been used for this purpose: parametric differential frequency generation,[7] semiconductor optical switching,[8] and the Kerr effect.[9] Two of them are utilized in the ATF laser system, and are described below.

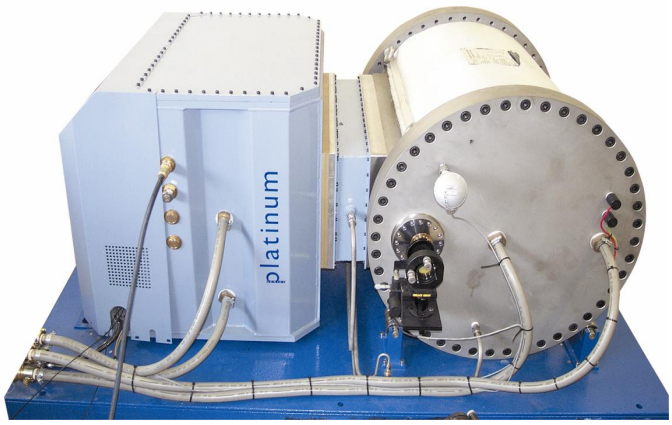

Figure 3: High-pressure UV-preionized CO_2 laser HP-5 manufactured by SDI Ltd. (Pretoria, S. Africa)

A semiconductor switch actually is a polished slab placed at the Brewster angle to the incident *p*-polarized CO_2 laser beam. A short-wavelength control laser, having photon energy above the band gap of a semiconductor, creates an electron-hole plasma in a surface layer. When the plasma reaches a critical density, which is 10^{19} cm^{-3} for λ=10 μm, the refractive index becomes imaginary, and the semiconductor slab, normally transparent to the IR radiation, briefly becomes a metal-like mirror. When germanium is used in the ATF laser system, this process requires 4 mJ/cm^2 of the λ=1 μm laser energy deposition onto the slab's surface. Using two sequential semiconductor switches allows to slice a pulse into lengths adjustable between the characteristic life-time of free carriers (200 ps for Ge) and down to the control pulse length.[10]

The optical Kerr gating technique is based on polarization rotation of the probe CO_2 laser pulse during the time when the Kerr medium is birefringent. In our case, birefringence is excited in the CS_2 liquid nonlinear medium by a 6-ps, 0.53-μm pump pulse, via molecular orientation. CS_2 is the best choice for the Kerr medium as it has a high nonlinear index of refraction, $n_2 = 0.33 \times 10^{-20} m^2/V^2$, a fast ~2-ps relaxation time[11], and transmits both the probe- and pump-laser beams well. A 2-cm long cell with CS_2 is placed between two crossed 10-μm polarizers. Thus, only a portion of the CO_2 pulse rotated by 90^0 inside the Kerr cell is transmitted through the cell. To achieve close to the maximum 50% of switching efficiency with a relatively small 3 mJ energy of the pump pulse, both the probe- and pump-beams were focused to ~ 1 mm diameter spots and combined in a collinear configuration over the entire length of the cell. The angle between the polarization of the probe and pump beams was set to 45^0.

As we saw from simulations, pulses as short as 1-ps can be amplified in the 10-atm laser without distortion. However, the short-wavelength pump pulse that controls Kerr-switching defines the initial duration of the CO_2 pulse, and the shortest pulse generated by the ATF laser system is a 6-ps second harmonic (SH) of Nd:YAG. To produce such a short pulse using the relatively long 14-ps fundamental YAG pulse requires using the following technique: We split a 30-mJ YAG pulse in two, rotate polarization for one component, and recombine them in a KD*P crystal with a certain delay between two split pulses. A 0.53-μm SH of the YAG is generated within the short overlap between two pulses, as depicted in Fig. 4.

Let us consider how the optical switches and laser amplifiers described above are assembled into a terawatt laser system (see Fig. 5). The front end of the ATF's CO_2 laser system is a hybrid 1-atm laser. i.e., a combination of a conventional grating-tuned TEA CO_2 oscillator operating at the TEM 00 mode (SDI Ltd., model WH-20) and a low-pressure "smoothing" discharge tube that eliminates longitudinal-mode beating in the output pulse envelope. To improve the contrast of a seed pulse entering the amplifiers, we use several consecutive pulse-chopping techniques. First, we cut a 10-ns pulse with a Pockels cell and a polarizer from the 150-ns oscillator output, and amplify this signal in a preamplifier that does not need to be under a critically high pressure. For this purpose, we use three passes in a 3-atm UV-preionized CO_2 laser with the active volume 2.5×5.0×120 cm^3 thus starting picosecond pulse switching from a low-background pulse at a 3-MW peak power.

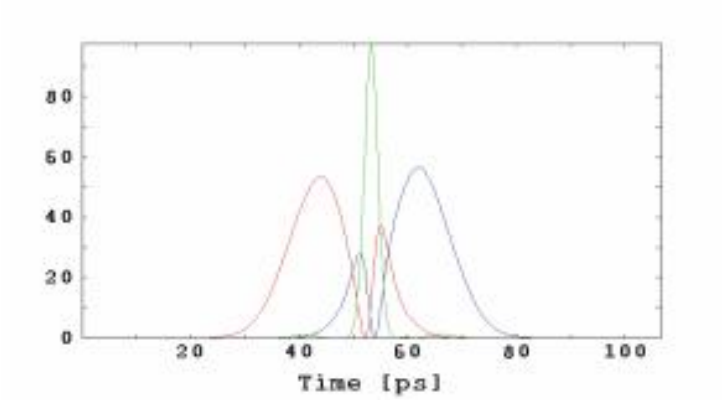

Figure 4: Simulated SH generation, λ=0.53 μm, (central narrow peak) in a 10-cm long KD*P crystal within overlap region of orthogonally polarized Nd:YAG pulses, λ=1.06 μm (broad side peaks).

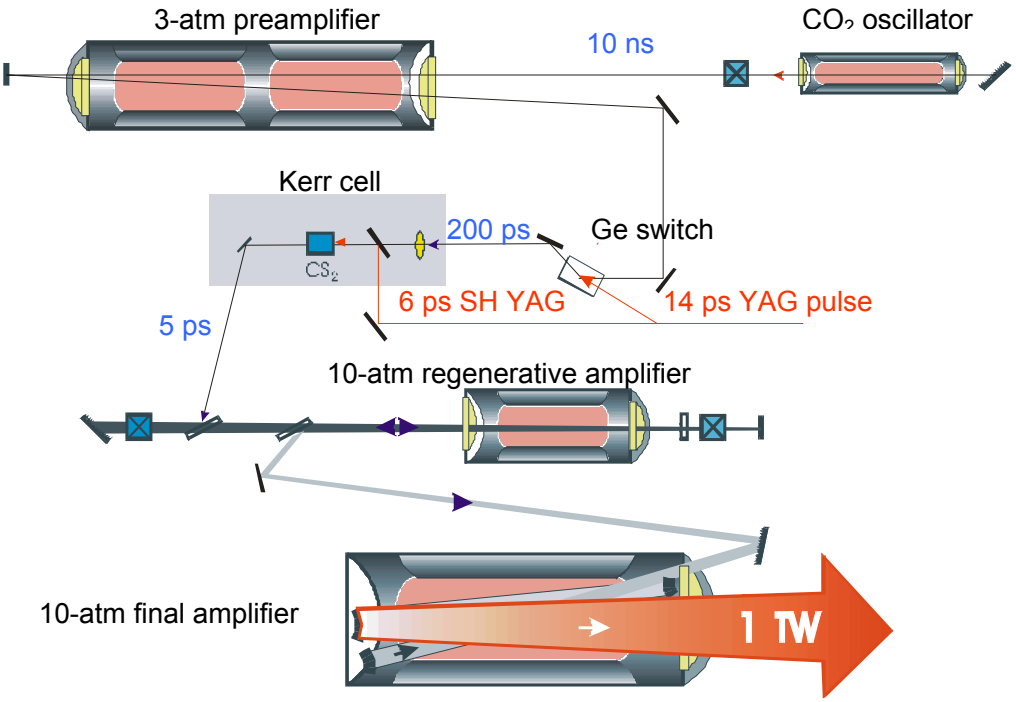

Figure 5: Principle optical scheme of the ATF CO_2 laser system

We separate a spent IR YAG beam after the SH generator and send it on a Ge optical switch to select a 200-ps, 10-μm pulse reflected from naturally decaying free carriers. After passing the additional wire-grid polarizer, the switched laser pulse has 10^4-power contrast over the 10-ns pedestal, and of $>10^6$ in respect to the longer 150-ns background. In addition, we time the semiconductor switching close to the leading front of the 10-ns pulse to reduce further an amplified pre-pulse that could be harmful for applications. In the next step, we slice a 6-ps CO_2 laser pulse in a Kerr switch using a SH of a Nd:YAG laser. After selecting and purifying with two sequential polarizers, the 6-ps pulse has a 10^3-power contrast over the 200-ps parent pulse. Again, by adjusting the delay of the control 0.53-μm pulse so it is within the rising edge of the 200-ps pulse, we preferentially amplify a short pulse with a low pre-pulse. Accordingly, we

generate a background-free, 2-μJ, 6-ps pure input pulse for amplification. Disengaging any stage of the described optical switching system, and observing practically no output laser energy after the amplifiers confirms the purity of the input signal.

The first in the high-pressure amplifier chain is a regenerative HP-5 amplifier. A seed CO_2 laser pulse is injected into the amplifier cavity by reflecting it from a thin-film polarizer (TFP). An input $\lambda/4$ Pockels cell, in combination with a $\lambda/4$ wave plate, traps the seed pulse for the controlled number of double passes inside the optical cavity until the laser power reaches several gigawatts. The optical damage threshold of Pockels cells prevents higher amplification. The second, output $\lambda/4$ Pockels cell releases the pulse by turning its polarization and reflecting the pulse from the output TFP.

Finally, a big-aperture high-pressure amplifier PITER-I boosts the laser-pulse's energy in 6 passes to 10 J and the peak power to ~1 TW. To arrange multiple passes, several externally controlled mirrors are assembled on the end flanges inside the high-pressure cell. On each pass, a laser beam and a corresponding mirror gradually expand in diameter until the output beam fills the 10-cm aperture window. This configuration sufficiently separates each reflection spatially to avoid their "cross-talking" and self-lasing, while keeping the intensity below the saturation level on each amplification pass.

For measuring pulse lengths, we use an autocorrelator based on the noncollinear SH generation in a $AgGaSe_2$ crystal. However, an autocorrelator cannot reveal the balance between the energy content in a short pulse and the relatively slow background. Thus, such measurements are not sufficient for calculating the peak power. Although the absence of any appreciable output energy with the seed pulse blocked strongly indicates that the amplifier energy is routed primarily into the picosecond pulse, we have also other indirect proof of the achievement of 1 TW peak power. This comes from applications of the PITER-I laser to strong-field experiments. An example that shows the real strength of PITER-I is the first demonstration of nonlinear Thomson scattering with a 15-ps laser pulse[2], and the recent enhancement of the x-ray yield to a new record of 6×10^8 photon/pulse after shortening the laser pulse to 6 ps (unpublished).

3. PROTON AND ION BEAMS RADIATED FROM A LASER TARGET

The 1 TW CO_2 laser power is sufficient to initiate a novel experiment on proton- and ion-acceleration from ablating thin foil and a gas jet. Generating intense proton- and ion-beams in high-intensity laser-matter interactions is an active area of research worldwide. State-of-the art experiments demonstrated collimated beams of protons and heavy ions at up to 100 MeV energy and an intensity two orders-of-magnitude larger than the intensity available at conventional accelerators.[3, 4] This may open applications of laser-driven sources in proton accelerators and for heavy-ion fusion. Possible uses in medicine include a compact ion beam injector for C-ion cancer therapy and the production of short-life-time radioisotopes for Positron Emission Tomography (PET).

So far, practically all research on laser ion acceleration has been conducted on multi-terawatt solid-state lasers at ~1 μm wavelength. The ATF's CO_2 laser can add an important new perspective to this development, not only because a CO_2 laser operating at 10 times longer wavelength will probe the acceleration mechanisms in the parameter domain presently unavailable, but also because it promises substantial enhancements in energy efficiency and particle yield. We discuss below the origin of these advantages.

Two mechanisms are most likely responsible for accelerating ions in the direction of the laser beam. One is Target Normal Sheath Acceleration (TNSA) [12] wherein electrons accelerated in a laser-plasma interaction to several MeV near the front surface of the target quickly move through the foil, producing a negatively charged cloud at its rear surface. The electric field due to charge separation at the rear surface reaches 10^{12} V/m, causing field ionization of external layers of atoms in the foil. The ions are pulled into vacuum by the electron-cloud charge. Depending upon the foil's material, proton- or various ion-beams can be produced with a high efficiency. The peak brightness of such beams may exceed that of conventional ion accelerators by orders of magnitude. An extremely high acceleration gradient results in low space-charge repulsion inside the ion/proton beam. Consequently, low emittance, good collimation, and even focusing of high-brightness heavy-particle beams become possible.

Simple considerations lead us to conclude that the efficiency of the acceleration by the TNSA mechanism scales favorably with the laser wavelength. Indeed, the key factors that determine the amount and spectra of accelerated ions are those of the relativistic electrons generated near the front surface of the target. An electron interacting with the electromagnetic wave acquires energy equal to $W_{osc}\sim I\times\lambda^2$ (see Eq. 1). Assuming that a laser is focused close to its

diffraction limit, electron energy depends on the laser power, regardless of the wavelength; the number of high-energy electrons is proportional to the interaction volume $\sim \lambda^3$ and to the critical plasma density $n_{cr} \sim \lambda^{-2}$. Therefore, the total energy in the electron ensemble grows linearly with the laser wavelength. We expect that the amount of secondary events (for example, accelerated ions) will also grow accordingly. In other words, at equal output power, a CO_2 laser might provide much higher yield of the accelerated particles than solid-state lasers. In this respect, a potential 10-J, 10-TW CO_2 laser becomes equivalent to a 100-J, multi-terawatt solid-state laser.

In addition to the higher particle yield, we expect a significant improvement in the beam's quality, such as collimation and monochromaticity. Let us illustrate this by the example of proton acceleration. Being the lightest ions, protons are always accelerated first from the surface and gain the highest energies. In all TNSA experiments so far, the registered proton spectra were quite broad due to the radial nonuniformity of the charge-separation field produced by the tightly focused laser beam.

A proposal to improve the quality of the spectrum[13, 14] is based on using structured targets with a small hydrogen-rich implant on the back surface of the target to enhance the proton yield in the central area of the accelerating field where it is nearly homogenous. As a result, the energy spectrum of the accelerated protons will be much narrower.

For a CO_2 laser, the focal spot size will be 10 times bigger than that of a solid-state laser. Consequently, a ten-fold improvement may be expected in the spectrum quality of the accelerated ion beam. To check this statement, we performed 3D PIC simulations for the following conditions: a laser pulse power P=20 TW, duration 600 fs and 60 fs for λ=10 μm and λ=1 μm, respectively, focal spot size 3 λ; target is a 5 μm-thick plasma layer consisting of high-Z ions of density n_e=100n_c. At the rear side of the plasma layer, we put a dot of hydrogen plasma of 20 μm radius and 0.25 μm thickness. Simulations show that the proton spectrum from a structured target is close to monoenergetic for a CO_2 laser only (see Fig. 6).

In the second mechanism, Shock Wave Acceleration (SWA), which usually requires larger laser energy and duration, a laser pulse drives a shock wave inside the over-dense plasma of the target. The shock wave pushes ions forward by the snowplow effect and, after approaching the back surface of the plasma foil, ejects energetic ions. These ions may then be further accelerated by the TNSA mechanism. Quasi-monoenergetic proton- and ion-beams with intensities up to 10^{22} sec^{-1} can be produced in this way.[15]

The picosecond laser-pulse duration typical for a CO_2 laser is particularly beneficial for the SWA mechanism. A larger spot size of CO_2 lasers at the maximum focusing might lead to smaller divergence of generated ion beams.

A qualitatively new potential advantage of a CO_2 laser is its ability to accelerate protons and ions in gas targets. Indeed, a normal air-pressure gas jet, when fully ionized, becomes a strongly over-dense plasma for a relatively long CO_2 wavelength. An important advantage is that a gas jet being easily restored after each laser shot.

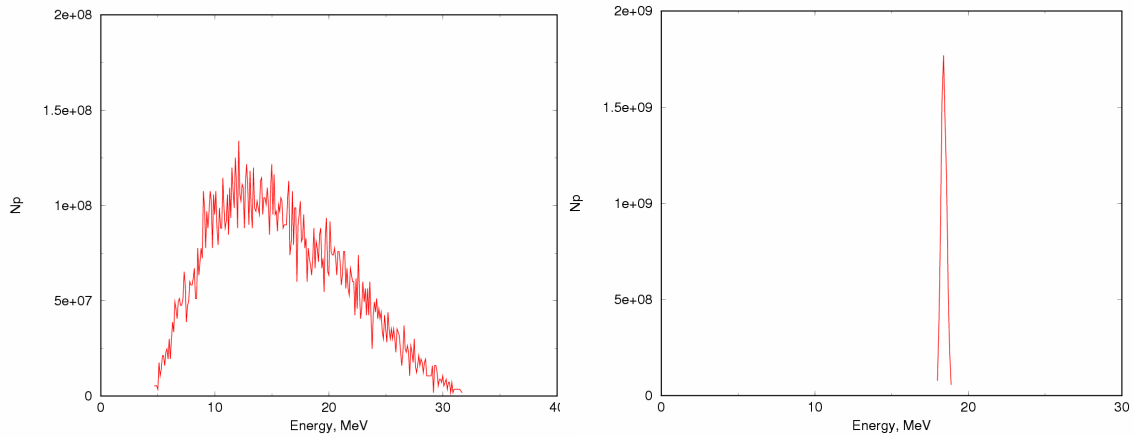

(a) (b)

Figure 6: Proton energy spectra simulated for a solid-state laser (a) and CO_2 laser (b) of the equivalent power.

Relativistically intense (a>1) lasers with λ~1 μm were used to accelerate ions to several MeV energies in gas jets.[16] However, the accelerated ions move radially from to the laser beam axis – a configuration ill suited for practical applications because the jet plasma is underdense for 1-μm radiation. When an intense laser pulse propagates in the underdense plasma, it is subject to relativistic self-channeling. The ponderomotive force of the laser pulse expels electrons out of the channel, generating a radial electrostatic field that accelerates the plasma ions via the radial Coulomb explosion.

The situation changes for a CO_2 laser. For its 10-μm radiation, a gas jet with readily available densities becomes significantly over-dense after multiple ionizations. Thus, we can apply the understanding developed for solid targets. It is clear that TNSA will not be very effective because the jet surface is not as sharply defined as it is for a solid target. Subsequently, the charge-separation field at the rear surface will not be nearly as strong. Therefore, SWA will become the main acceleration mechanism. 1D PIC simulations predict up to 10^{10} protons at ~10 MeV with the 10-J CO_2 laser, which is on a par with the results from solid targets.

To conduct the proton-acceleration experiment, we assembled a vacuum chamber (Fig. 7) where a CO_2 laser pulse of up to 10 J energy is focused by a short-focal-length parabolic mirror into the diffraction-limited spot on a target foil that will be complemented later by a gas jet. Intra-cavity diagnostics includes a stack of radiochromic films and a Faraday cup. The permanent magnet ion spectrometer will allow imaging of the ion beam at different energies. Transmutation of a ^{48}Ti catcher foil by a (p,n) reaction to the ^{48}V isotope can be used as a complementary detector of protons above 5 MeV.

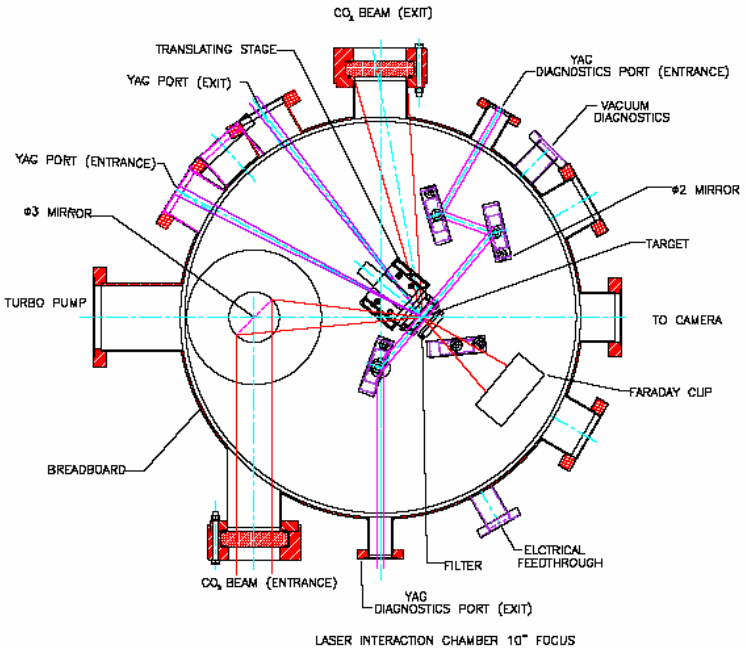

Figure 7: Diagram of the proton- and ion acceleration experiment assembled at ATF.

4. PETAWATT AND FEMTOSECOND FRONTIERS OF CO_2 LASER TECHNOLOGY

Finally, we address prospects of ultra-fast CO_2 technology on a bigger scale. Can we push CO_2 lasers to the few-cycles limit? Only the control pulse length limits a semiconductor's switching speed. For example, Corkum reported 130-fs (4 cycles) CO_2 pulses sliced with a 70-fs dye laser .[17]

Another proposal is to convert the energy of a nanosecond CO_2 pump pulse into the frequency-downshifted short seed pulse via Raman scattering in the resonance plasma.[18] An optimum configuration includes a 1-ns, 5-J pump pulse at λ=9 μm, and a 10-ps seed pulse at λ=10 μm counterpropagating in the n_e=10^{17} cm^{-3} plasma that has a wake in resonance with the beat frequency between the laser pulses. Simulations show that Raman scattering not only adds to the short

pulse's intensity that acquires multi-terawatt power, but simultaneously compresses it to a single cycle (30 fs for 10 μm radiation).

A different approach to pulse shortening based on a frequency chirp in the laser-ionized gas was practically implemented at the UCLA's NEPTUNE laboratory. This laboratory is equipped with a 3-atm, *e*-beam pumped, 30-cm aperture CO_2 amplifier MARS. The 3-atm pressure sets the 200 ps minimum to the transform-limited pulse. Transmitting a focused laser pulse through a gas cell changes the refraction index due to ionization

$$\eta(x,t) = \sqrt{1 - n_e(x,t)/n_{cr}} \tag{6}$$

with the subsequent frequency chirp along the laser pulse

$$\Delta\omega = \frac{\pi n_e^0}{\lambda n_{cr}} \frac{\partial}{\partial t} \int n_e(t,x) dx \ . \tag{7}$$

When the pulse is returned back into the amplifier, the frequency-chirped tail is filtered out by a narrow gain profile. In this way, the output pulse was compressed from 200 ps to 40 ps.[19] Corkum earlier suggested employing similar chirping in a gas with a subsequent negative dispersion material ($d\eta/d\omega < 0$) to compress the initial 1-2 ps pulses down to 100-150 fs.

There are several ideas for a broadband CO_2 laser medium able to amplify femtosecond pulses. An alternative for, or complimentary to the pressure-broadening approach for gain smoothing is by multiplying the number of rotational lines in a mixture of CO_2 isotopes. Then the rotational lines overlap at a lower pressure. For example, transitions 10P(26)-10P(31) of the $^{12}C^{18}O_2$ molecule are shifted by a half of the interline spacing (~0.9 cm^{-1}) from the lines 10P(18)-10P(24) of $^{12}C^{16}O_2$ molecule. Such a mixture allows reducing the working pressure twofold to produce a similarly smooth spectrum relative to a regular gas. In addition, replacing just one of the oxygen nuclei by that of a different isotope $^{12}C^{18}O^{16}O$ destroys the symmetry of the CO_2 molecule. Consequently, twice as many V-R transitions are allowed, and the gain spectrum becomes twice as dense as that of a regular CO_2 molecule. If we consider a balanced mixture $^{12}C^{16}O_2$:$^{12}C^{16}O^{18}O$:$^{12}C^{18}O_2$=1:2:1, then, due to isotopic shifts, the combined spectrum will have approximately a factor-of-four denser rotational line structure relative to a regular CO_2 molecule. Further expansion can be achieved of the quasi-continuum in the CO_2 gain up to a total of 7 THz composed of P- and R- branches of the 9-μm and 10-μm bands by mixing CO_2 isotopes using possible combinations of atoms ^{16}O, ^{18}O, ^{12}C, ^{13}C, and ^{14}C. This way, 200-fs CO_2 pulses (about 7 laser cycles) can be amplified directly in the gas laser medium.[20]

UCLA researchers observed also the effect of a power- or Stark-broadening $\Delta\nu_s = \mu E/\hbar$ (=37 GHz @ I=10^{10} W/cm^2) that, similar to the pressure broadening, allows bridges to form between rotational lines to provide sufficient bandwidth for the 1-ps pulse amplification.[19] Simulations show[21] that, with the 1-TW picosecond pulse sent into the MARS-type amplifier, close to 1 PW can be extracted after four passes (~ 10 m propagation) and a beam expansion to the 30 cm aperture.

Limitations to the repetition rate of the high-pressure lasers are primarily technical ones, due to the required high energy loading of ~100 J/*l* atm into the medium, and the restricted capabilities of high-voltage commutation devices, such as thyrotrons or spark gaps. Laser gas recovery between the discharge shots is another factor to be considered. The existing terawatt CO_2 lasers, such as PITER-I, are not designed for high-repetition-rate operation. The repetition rate of such a laser might be increased to ~ 10 Hz by a straightforward upgrade of the DC power supply, fast gas circulation through the catalytic converter, fast vacuum pumping of the x-ray tube, and by building a pulse-forming network that uses semiconductor high-voltage switches.

A high-pressure CO_2 laser scheme alternative to discharge pumping is being explored; it has particularly good potential for progressing to a high-output energy and a repetition rate. According to this scheme, chemical energy released in burning hydrogen and fluorine, which results in lasing on the HF molecule, can be optically transferred to CO_2 molecules.[22] This process has nearly 100% quantum efficiency and can be carried out at a 10-20 atm pressure, sufficient for picosecond pulse amplification. The abundance of the deposited energy per liter of the laser's volume affords a very high optical gain of 10%/cm permitting a much more compact amplifier than one pumped with the electric discharge.

Another possibility worth exploring is pure chemical pumping via direct energy transfer from DF* to CO_2 in reactions

$$F+D_2=DF^*+D, \quad D+F_2=DF^*+F, \quad DF^* + CO_2 = DF + CO_2^*.$$

5. CONCLUSIONS

The BNL's picosecond terawatt CO_2 laser PITER-I is operated as a user's facility for advanced high-energy physics applications where a CO_2 laser offers a fundamental advantage due to the λ^2-proportional ponderomotive potential. Proton- and ion-acceleration are among the experiments where new breakthrough results are expected soon. In a longer run, CO_2 lasers, being the most robust and energy-efficient devices, may become the choice drivers for future high-repetition-rate, high-average-power relativistic ion- and proton-beam sources.

A prospective 1 PW λ=10 μm laser beam focused to the diffraction limit will produce a field with a=70; with this, we may realize a high-flux GeV ion injector, direct ponderomotive acceleration of electrons in a laser focus, produce and study Unruch radiation, and other highly relativistic processes.

ACKNOWLEDGEMENTS

The authors wish to thank L. Botha (SDI Ltd.) and I. Meshkovsky (Optoel Co.) for their active role in customizing a CO_2 laser technology to the ATF requirements, M. Roth (Technische Universität, Darmstadt**)** for the support in initiating the ATF's ion acceleration experiment, and A. Woodhead (BNL) for technical help in preparing this paper. The work was performed under the auspices of the U.S. Department of Energy contract number DE-AC02-98CH10886.

REFERENCES

1. I.V. Pogorelsky, I. Ben-Zvi, T. Hirose, S. Kashiwagi, V. Yakimenko, K. Kusche, P. Siddons , J. Skaritka, T. Kumita, A. Tsunemi, T. Omori, J. Urakawa, M.Washio, K. Yokoya, T. Okugi, Y. Liu, P. He, and D. Cline, *Phys. Rev. ST - AB* **3**, 090702 (2000)
2. M. Babzien, I. Ben-Zvi, K. Kusche, I. V. Pavlishin, I. V. Pogorelsky, D. P. Siddons, V. Yakimenko, D. Cline, F. Zhou, T. Hirose, Y. Kamiya, T. Kumita, T. Omori, J. Urakawa, and K. Yokoya, *Phys. Rev. Lett.* **96**, 054802 (2006)
3. K. Krushelnick, E. L. Clark, F. N. Beg, A. E. Dangor, Z Najmudin, P. A. Norreys, M. Wei1, and M. Zepf, *Plasma Phys. Control. Fusion* **47**, B451 (2005).
4. M. Roth, A. Blazevic, M. Geissel, T. Schlegel, T. E. Cowan, M. Allen, J. C. Gauthier, P. Audebert, J. Fuchs, J. Meyer-ter-Vehn, M. Hagelich, S. Karsh, and A. Pukhov, *Phys. Rev. ST - AB* **5,** 061301 (2002).
5. V.T. Platonenko and V.D. Taranukhin, *Sov. J. Quant. Electron*. **13**, 1459 (1983)
6. I. V. Pogorelsky, I. Ben-Zvi, M. Babzien, K. Kusche, J. Skaritka, I. Meshkovsky, A Dublov, V. Lekomtsev, I. Pavlishin, Yu. Boloshin, and G. Deineko, Laser Optics '98, St. Petersburg, June 22-26 1998, "Superstrong Laser Fields and Applications", *Proc. of SPIE* **3683**, 15 (1999)
7. T. Elsaesser, AQ. Seilmeir and W. Kaiser, *Opt. Commun.* **44**, 293 (1983)
8. A.J. Alcock and P.B. Corkum, *Can. J. Phys.* **57**, 1280 (1979)
9. C. V. Filip, R. Narang, S. Ya. Tochitsky, C. E. Clayton, and C. Joshi, *Appl. Optics* **41**, 3743 (2002)
10. P.B. Corkum, *IEEE J. Quantum. Electron* **QE-21**, 216 (1985)
11. M.A. Duguay and J.W. Hansen, *Appl. Phys. Lett.* **15**, 192 (1969)
12. J. Fuchs, Y. Sentoku, S. Karsch, J. Cobble, P. Audebert, A. Kemp, A. Nikroo, P. Antici, E. Brambrink, A. Blazevic, E. M. Campbell,1 J. C. Fernandez, J.-C. Gauthier, M. Geissel, M. Hegelich, H. Pepin, H. Popescu, N. Renard-LeGalloudec, M. Roth, J. Schreiber, R. Stephens, and T. E. Cowan, *Phys. Rev. Lett*. **94**, 045004 (2005)

13. T. Esirkepov, et al., *Phys. Pev. Lett.* **89**, 175003 (2002)
14. H. Schwoerer, S. Pfotenhauer, O. Jäckel, K.-U. Amthor, B. Liesfeld, W. Ziegler, R. Sauerbrey, K. W. D. Ledingham, and T. Esirkepov, *Nature* **439**, 445 (2006).
15. A. Zhidkov, M. Uesaka, A. Sasaki, H. Daido, *Phys. Rev. Lett*. **89**, 215002 (2002); A. A. Andreev, A. Zhidkov, A. Sasaki, and K. Y. Platonov, *Plasma Phys. Control. Fusion* **44**, 1243 (2002)
16. T. Hosokai, K. Kinoshita, T. Watanabe, K. Yoshii, T. Ueda, A. Zhidkov, M. Uesaka, H. Kotaki, M. Kando, K. Nakajima, *AIP Conf. Proc.* **647**, 628 (2002).
17. C. Rolland and P.B. Corkum, *J. Opt. Soc. Am.* B **3**, 1625 (1986)
18. V.M. Malkin, G. Shvets, and N.J. Fish, *Phys. Rev. Lett* **82**, 4448 (1999)
19. S. Yu. Tochitsky, R. Narang. C. Filip, C. E. Clayton, K. A. Mash, and C. Joshi, *Optics Letts*. **24**, 1717 (1999)
20. Z.A. Biglov and V.M. Gordienko, *Current Problems in Laser Physics* **4**, Moscow, 1991
21. I. V. Pogorelsky, *Proceedings of Lasers'2001*, December 3-7, 2001, Tucson, AZ, STS Press, McLean, VA, 1 (2002)
22. B.S. Alexandrov, A.V. Arsenjev, M.A. Azarov, V.A. Drozdov, V.I. Mashendzhinov, V.E. Revich, and G.A. Troshchinenko, *Proc. SPIE* **4184**, 315 (2001)